

CrossMark
click for updatesCite this: *RSC Adv.*, 2015, 5, 42354

Efficient near-infrared-emitting cationic iridium complexes based on highly conjugated cyclometalated benzo[*g*]phthalazine derivatives†

Lijun Xin,^{ab} Jie Xue,^b Gangtie Lei^{*a} and Juan Qiao^{*b}

Two near-infrared- (NIR-) emitting cationic iridium(III) complexes, $[\text{Ir}(\text{dpbpa})_2(\text{Bphen})]^+\text{PF}_6^-$ (**1**) and $[\text{Ir}(\text{dtbpa})_2(\text{Bphen})]^+\text{PF}_6^-$ (**2**), were rationally designed and synthesized, where dpbpa, dtbpa, and Bphen represent 1,4-diphenylbenzo[*g*]phthalazine, 1,4-di(thiophen-2-yl)benzo[*g*]phthalazine and 4,7-diphenyl-1,10-phenanthroline, respectively. By using highly conjugated cyclometalated benzo[*g*]phthalazine ligands, these two complexes exhibited a significantly large red shift in wavelength to the truly NIR region with maximum peaks at 715 nm for **1** and 775 nm for **2**. Complex **1** exhibited unexpectedly improved quantum efficiency up to 6.1% in the solid films. Based on these solution-processable phosphors, NIR organic-light-emitting devices (OLEDs) have been fabricated and demonstrated negligible efficiency roll-off with nearly constant external quantum efficiency around 0.5% over a wide range of current density of 1–100 mA cm⁻². Density functional theory calculations were performed to discover that the newly cyclometalated benzo[*g*]phthalazine ligands have several areas of superiority over the previous benzo[*g*]quinoline ligands in views of stronger Ir–N bonds, smaller chelate congestion, higher electron-accepting ability, thus improving the overall phosphorescence of the corresponding iridium complexes in the NIR region.

Received 14th March 2015
Accepted 5th May 2015

DOI: 10.1039/c5ra04511h

www.rsc.org/advances

Introduction

In recent years, near-infrared- (NIR-) emitting materials have aroused rapidly growing attention because of their emerging applications in night-vision and/or information-secured displays, bio-imaging and diagnosis, chemosensors, optical communication, and phototherapy, *etc.*^{1–6} To date, several kinds of pure organic compounds and metal-complexes have been reported as organic NIR emitting materials, such as organic small-molecules,^{1,2} lanthanide complexes,^{5,6} conjugated polymers,^{7–9} metalloporphyrins^{10–12} and other transition-metal complexes.^{3,4} Compared with traditional fluorescent materials, phosphorescent transition-metal complexes offer several important advantages as NIR dyes.^{3,4} For NIR organic-light-emitting devices (OLEDs), transition-metal complexes can harvest both singlet and triplet excitons as light and theoretically achieve nearly 100% internal quantum efficiency. Most notably, platinum metal complexes have demonstrated the most efficient

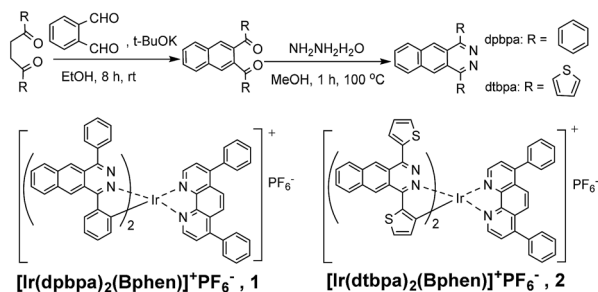
NIR-OLEDs with the record maximum external quantum efficiencies (EQEs) up to ~14.5% at ~700 nm,¹³ and ~9% in the 750–800 nm range¹² and 4% in the 850–900 nm range.¹¹ However, those NIR-OLEDs based on platinum metalloporphyrins generally suffer from severe efficiency roll-off with increasing current density, which could be mainly ascribed to the easy aggregation of the planar-square configuration and the intrinsic long phosphorescence lifetime of the complexes.^{11–13} In comparison, the other transition-metal complexes with octahedral configurations (*e.g.*, containing Ir³⁺, Os³⁺, Re³⁺) would help to alleviate the efficiency roll-off in the corresponding OLEDs, although with relatively low efficiencies in NIR region.^{14–20} Since 2009, we have designed and synthesized a series of NIR-emitting iridium complexes based on benzo[*g*]quinoline and benzo[*g*]quinoxaline derivatives, which exhibited desirable emission covering 690–1000 nm and reasonable quantum efficiency around 3% in solutions.^{19–22} Of particular concern is that the NIR-OLEDs based on those Ir(III) complexes demonstrated negligible efficiency roll-off at high current density.^{19–21}

However, it is still quite challenging to design high-efficiency NIR emitting phosphors, since their photoluminescence quantum yields (PLQY) tend to decrease with an increase in the emission wavelength according to the energy gap law. In this work, we continue our efforts in developing highly efficient NIR emitting Ir(III) phosphors. To loosen the steric congestion from the previous benzo[*g*]quinoline ligand and further improve the overall phosphorescence of iridium complexes in NIR region, we

^aKey Laboratory of Environmentally Friendly Chemistry and Applications of Ministry of Education, College of Chemistry, Xiangtan University, Hunan 411105, China. E-mail: lgt@xtu.edu.cn

^bKey Lab of Organic Optoelectronics and Molecular Engineering of Ministry of Education, Department of Chemistry, Tsinghua University, Beijing 100084, China. E-mail: qjuan@mail.tsinghua.edu.cn

† Electronic supplementary information (ESI) available. See DOI: 10.1039/c5ra04511h



Scheme 1 The synthetic route of the cyclometalated ligand dpbpa, dtbpa and the molecular structures of the iridium(III) complexes.

designed two novel cyclometalated benzo[*g*]phthalazine derivatives, 1,4-diphenylbenzo[*g*]phthalazine (dpbpa) and 1,4-di(thiophen-2-yl)benzo[*g*]phthalazine (dtbpa) and synthesized the corresponding iridium complexes with the diimine ancillary ligand (Scheme 1): $[\text{Ir}(\text{dpbpa})_2(\text{Bphen})]^+\text{PF}_6^-$ (**1**) and $[\text{Ir}(\text{dtbpa})_2(\text{Bphen})]^+\text{PF}_6^-$ (**2**) (Bphen = 4,7-diphenyl-1,10-phenanthroline). Herein, we systematically studied their molecular and electronic structures, photophysical and electrochemical properties, and the NIR-OLEDs performances, particularly in comparison with the previous benzo[*g*]quinoline based complexes.²² The density-functional theory calculations were also performed to gain a better understanding the relationship between the structure of cyclometalated ligand and NIR emitting properties of these materials. It was found that the newly cyclometalated benzo[*g*]phthalazine ligands have several superiority over the previous benzo[*g*]quinoline ligands in views of easy synthesis, stronger Ir–N bonds, smaller chelate congestion and higher electron-accepting ability, thus providing the corresponding complexes with truly NIR emission up to 788 nm and notable PLQY up to 6.1% due to the desirable MLCT (metal-to-ligand charge transfer) mixed with ILCT (intraligand charge transfer).

Experimental section

General information and characterization

¹H NMR spectra were collected using JEOL JNM-ECA400NMR (400 MHz) NMR spectrometers with tetramethylsilane as the internal standard. Mass spectra were recorded on a Thermo-Electron Corporation Finnigan LTQ mass spectrometer (ESI-MS) and LCMS-IT/TOF (HRMS). Elemental analysis was performed on an Elementar Vario EL CHN elemental analyzer. Steady-state absorption and photoluminescence (PL) spectra were carried out on an Agilent 8453 UV-vis spectrophotometer and an Edinburgh FLSP920 spectrofluorometer, respectively. The photoluminescence quantum yield (PLQY) was measured in degassed CH₂Cl₂ solutions and 5 wt% doped poly(methyl methacrylate) (PMMA) films with an absolute PL quantum yield spectrometer (C9920-02, Hamamatsu photonics k. k.). Cyclic voltammetry measurements were performed on a Princeton Applied Research potentiostat/galvanostat model 283 voltammetric analyzer in anhydrous acetonitrile solutions (10^{−3} M) at a scan rate of 150 mV s^{−1} at room temperature. The solutions were bubbled with argon for 15 min before measurements. The

supporting electrolyte was tetra-*n*-butylammonium perchlorate (0.1 M), and ferrocene was selected as the internal standard.

Materials and synthesis

All reagents and starting materials are commercially available and were used without further purification. All procedures involving IrCl₃·*x*H₂O were carried out under a nitrogen atmosphere.

Synthesis of 1,4-diphenylbenzo[*g*]phthalazine (dpbpa). dpbpa was prepared according to the literature methods.^{23,24} Briefly, *t*-BuOK was slowly added into the hot ethanolic solution of 1,4-diphenylbutane-1,4-dione (8 mmol, 1.9 g) and phthalaldehyde (8 mmol, 1.0 g) and the solution was stirred for 8 h at room temperature. Upon cooling, the mixture was filtered and the residue was washed with methanol to afford naphthalene-2,3-diylbis(phenylmethanone) (2.4 g). Then, a hot methanolic solution of naphthalene-2,3-diylbis(phenylmethanone) was dropped in excess hydrazine hydrate and the mixture was refluxed at 70 °C for 1 hour. After being cooled to room temperature, the mixture was filtered and the residue was washed with methanol to give bright yellow solid as the ligand dpbpa (2.4 g, yield 90%). ¹H NMR (400 MHz, CDCl₃): δ 8.71 (s, 2H), 8.07 (dd, *J* = 6.4, 3.0 Hz, 2H), 7.98–7.83 (m, 4H), 7.72–7.55 (m, 8H). ESI-MS (*m/z*): 333 [M + H]⁺. HRMS (ESI⁺): calcd for C₂₄H₁₆N₂: 333.1386 [M + H]⁺, found 333.1381 [M + H]⁺. Anal. calcd (%) for C₂₄H₁₆N₂: C, 86.72; H, 4.85; N, 8.43. Found: C, 86.21; H, 4.48; N, 8.68%.

Synthesis of 1,4-di(thiophen-2-yl)benzo[*g*]phthalazine (dtbpa). The synthesis of dtbpa was similar to that of dpbpa except that 1,4-diphenylbutane-1,4-dione was replaced with 1,4-di(thiophen-2-yl)butane-1,4-dione. The target ligand dtbpa was received as yellow solid (3 g, yield 90%). ¹H NMR (600 MHz, DMSO-*d*₆) δ 9.29 (s, 2H), 8.46 (dd, *J* = 6.4, 3.3 Hz, 2H), 8.17–8.10 (m, 2H), 8.00–7.90 (m, 2H), 7.82 (dd, *J* = 6.5, 3.2 Hz, 2H), 7.43 (dd, *J* = 5.0, 3.7 Hz, 2H). ESI-MS (*m/z*): 345 [M + H]⁺. HRMS (ESI⁺): calcd for C₂₀H₁₂N₂S₂: 345.0515 [M + H]⁺, found: 345.0514 [M + H]⁺. mp: 258–260 °C. Anal. calcd (%) for C₂₀H₁₂N₂S₂: C, 69.74; H, 3.51; N, 8.13. Found: C, 69.37; H, 3.45; N, 7.78%.

Synthesis of complexes 1 and 2. These two complexes were prepared in a conventional two-step procedure according to our previous work.²⁰

$[\text{Ir}(\text{dpbpa})_2(\text{Bphen})]^+\text{PF}_6^-$ (**1**): black solid. (0.81 g yield 40%). ¹H NMR (600 MHz, CDCl₃): δ 9.60 (d, *J* = 10.4 Hz, 2H), 8.75 (s, 2H), 8.60 (d, *J* = 7.9 Hz, 2H), 8.48 (d, *J* = 5.2 Hz, 2H), 8.29 (d, *J* = 8.4 Hz, 2H), 8.09 (d, *J* = 8.5 Hz, 2H), 8.01 (s, 2H), 7.81–7.78 (m, 2H), 7.75–7.71 (m, 2H), 7.67 (d, *J* = 5.2 Hz, 2H), 7.60–7.55 (m, 7H), 7.49 (t, *J* = 7.5 Hz, 3H), 7.45 (d, *J* = 7.6 Hz, 4H), 7.35 (dt, *J* = 29.2, 7.5 Hz, 8H), 7.09 (t, *J* = 7.4 Hz, 2H), 6.76 (d, *J* = 7.5 Hz, 2H). ESI-MS (*m/z*): 1187 [M – PF₆]⁺. HRMS (ESI⁺): calcd for IrC₇₂H₄₆N₆⁺: 1187.3420 [M – PF₆]⁺, found 1187.3416 [M – PF₆]⁺. Anal. calcd (%) for IrC₇₂H₄₆N₆PF₆: C, 64.91; H, 3.48; N, 6.31. Found: C, 63.36; H, 3.20; N, 5.70%.

$[\text{Ir}(\text{dtbpa})_2(\text{Bphen})]^+\text{PF}_6^-$ (**2**): black solid. (1.47 g, yield 50%). ¹H NMR (600 MHz, CD₂Cl₂): δ 9.44 (d, *J* = 19.4 Hz, 2), 9.10 (d, *J* = 14.3 Hz, 2H), 8.52–8.44 (m, 2H), 8.34 (d, *J* = 8.4 Hz, 2H), 8.20 (d, *J* = 8.4 Hz, 2H), 8.11 (d, *J* = 7.6 Hz, 2H), 7.84–7.80 (m, 4H), 7.79–

7.75 (m, 4H), 7.70 (t, $J = 5.1$ Hz, 2H), 7.64–7.60 (m, 6H), 7.58–7.54 (m, 4H), 7.40–7.35 (m, 2H), 7.23–7.16 (m, 2H), 6.85–6.80 (m, 2H). ESI-MS (m/z): 1211 [$M - PF_6$]⁺. HRMS (ESI⁺): calcd for $C_{64}H_{38}IrN_6S_4$ ⁺: 1211.1669 [$M - PF_6$]⁺, found 1211.1174 [$M - PF_6$]⁺. Anal. calcd (%) for $IrC_{64}H_{38}N_6S_4PF_6$: C, 56.67; H, 2.82; N, 6.20. Found: C, 56.51; H, 2.60; N, 6.12%.

Quantum chemical calculation

All calculations were carried out with Gaussian 03 software package using a spin-restricted formalism.²⁵ The ground and excited electronic states of the complexes were calculated using density functional theory (DFT) and time-dependent DFT (TD-DFT) at the B3LYP level.^{26,27} The standard valence double- ξ polarized basis sets were used for C, H and N (6-31G*) and Ir (LANL2DZ). An effective core potential (ECP) replaces the inner core electrons of Ir, leaving the outer core [(5s)²(5p)⁶] electrons and the (5d)⁶ valence electrons of Ir(III). The geometries of the singlet ground state (S_0) were fully optimized without symmetry constraints at the N–N *trans* type, which was reported as the most stable structural isomer for iridium(III) complexes with the diimine ligand. The electron density diagrams of molecular orbitals were obtained with the ChemBioOffice 2010 software.

Fabrication and characterization of OLEDs

Before device fabrication, the prepatterned indium tin oxide (ITO) glass substrates were carefully cleaned and treated by an UV-ozone for 6 min. Then 40–50 nm poly(3,4-ethylenedioxythiophene) (PEDOT:PSS, Bayer Baytron P8000) used as a hole-injecting layer was spin-coated on the ITO substrate and baked at 200 °C for 10 min in a nitrogen glovebox. The emitting layer was spin-coated onto the PEDOT:PSS-coated substrate from 1,2-dichloroethane solutions and then annealed at 80 °C for 30 min to remove the solvent residue. Afterwards, the substrates were transferred into an evaporation chamber integrated with the glovebox for the deposition of electron-transporting layer and metal cathode. 2,2',2''-(1,3,5-Benzene-triyl)tris-(1-phenyl-1*H*-benzimidazole) (TPBI) was evaporated as the electron-transporting layer at a rate of 0.5–1 Å s⁻¹ under a pressure of 4 × 10⁻⁴ Pa. Finally, the Cs₂CO₃/Al bilayer cathode was evaporated at rates of 0.2 Å s⁻¹ and 5–10 Å s⁻¹, respectively, under a base pressure of 4 × 10⁻⁴ Pa. The current density–voltage characteristics were measured with a Keithley 4200 semiconductor characterization system, and optical power was recorded on a Newport 1936-C power meter coupled to a calibrated Newport 918D-UV-OD3 detector with a spectral response range from 200 to 1100 nm. The EQE (η_{ext}) was derived on the basis of the generally-adopted methods.^{20,21} Electrophosphorescent spectra were collected with a Jobin Yvon FluoroMax-3 fluorospectrophotometer. All measurements were carried out in air at room temperature with encapsulation.

Results and discussion

Design, synthesis and characterization

Substituted quinoline, isoquinoline and phthalazine derivatives are well-known cyclometalated ligands to obtain highly efficient

orange to red emitting iridium complexes.^{4,28–33} For iridium complexes, expanding π -conjugation length in the cyclometalated C[^]N ligands has been demonstrated as one of the most effective means to reduce the emission energy into NIR region.^{3,4} However, it is intrinsically quite challenging to design high-efficiency NIR emitting phosphors in accordance with the energy gap law. In our previous work, we designed cyclometalated benzo[*g*]quinoline and benzo[*g*]quinoxaline ligands with fused aromatic rings and realized efficient NIR-emitting iridium complexes.^{19–22} To loosen the steric congestion from those bulky ligands and further improve the PLQY of the complexes in NIR region, we designed two novel cyclometalated ligands based on benzo[*g*]phthalazine and synthesized the corresponding iridium complexes with the diimine ancillary ligand. Scheme 1 depicted the synthesis of the benzo[*g*]phthalazine ligands and the molecular structures of the corresponding complexes **1** and **2**. The ligand dpbpa and dtbpa were readily obtained by two steps with a high yield of 90% according to the literature methods.^{23,24} The iridium complexes were obtained *via* treatment of the corresponding chloride-bridged dimer precursor with Bphen as the ancillary ligand, followed by a counterion exchange reaction from Cl⁻ to PF₆⁻. The NMR spectra of the chloride-bridged dimer and the final complexes are both consistent with the cyclometalated ligands being in a C–C *cis*, N–N *trans* configuration.

Photophysical properties

Photophysical properties of complexes **1** and **2** were studied in degassed CH₂Cl₂ solutions and thin films. Fig. 1 depicts both UV-vis absorption and PL spectra of these two complexes in degassed CH₂Cl₂ solutions at room temperature. These two complexes exhibit similar absorption peaks from 300 to 600 nm. The intense short-wavelength absorption bands below 350 nm could be ascribed to spin-allowed intraligand $\pi \rightarrow \pi^*$ transitions, while the relatively long-wavelength absorption above 350 nm could be assigned to mixed transitions of spin-allowed ¹MLCT and spin-forbidden ³MLCT (singlet and triplet metal-to-ligand charge transfer). Because of thiophen-2-yl instead of phenyl in the cyclometalated ligands, those charge transfer transitions of complex **2** give a little bit red-shifted absorption bands around 454, 535 nm *versus* complex **1**. As shown in Fig. 1, the whole PL spectra of these two complexes fall in the NIR region, with a significantly red-shift around 100 nm compared with the red-emitting iridium complexes (625 nm) with substituted cyclometalated phenylphthalazine ligand.³³ Complex **1** exhibits a clearly resolved emission profiles with two strong emission peaks at 715 nm and 788 nm. In comparison, complex **2** further gives over 60 nm red-shifted emission peaks at 775 nm due to the thiophen-2-yl instead of phenyl in the cyclometalated ligands.

The detailed photophysical properties of these two complexes were summarized in Table 1. In degassed CH₂Cl₂ solutions, complex **1** exhibits modest PLQY of 3.1% and a relatively long emission lifetime of 0.79 μ s. We deduced the radiative decay rate (k_r) of complex **1** to be 3.9 × 10⁴ s⁻¹, which is comparable to that of our previously reported NIR-emitting

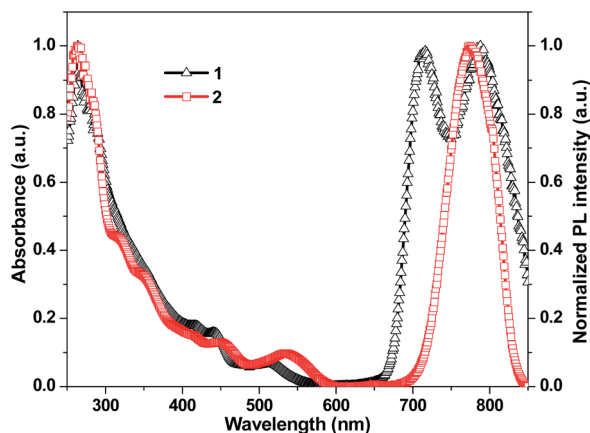


Fig. 1 The room-temperature UV-vis absorption (left) and photoluminescence spectra (right, corrected to 850 nm corresponding to the instrument limit) of complexes **1** and **2** in degassed CH_2Cl_2 solutions (10^{-5} M). The excitation wavelength was 440 nm.

iridium complexes based on cyclometalated benzo[*g*]quinoline so the k_f is estimated to be $8.78 \times 10^4 \text{ s}^{-1}$. When doped in PMMA films (5 wt%), both complexes exhibit similar emission profile to those in solutions, but a little blue-shifted (~ 10 nm) emission peaks and markedly improved PLQYs due to an increased rigidity in solid films and the polarity difference of the solvent/medium (Fig. S1 in the ESI[†]). The PLQYs of the PMMA doped films are significantly increased compared with those in solutions. In particular, the PLQY of complex **1** reaches 6.1% in the 5 wt% doped PMMA film, nearly twice than that in solution. It could be explained by the efficient suppression of non-radiative decay pathways in the rigid polymer matrix.

Electrochemical properties

The electrochemical properties of these two complexes were investigated by cyclic voltammetry in anhydrous CH_3CN solution. As shown in Fig. 2, both complexes are electrochemically active and undergo similar electrochemical characteristics with one reversible oxidation process and two reversible reduction processes in CH_3CN solution. Two reversible reduction processes occurred at half-wave potentials of -1.40 V and -1.55 V and for **1**, -1.39 V and -1.55 V for **2**, while the

reversible oxidation process arose at half-wave potentials of 1.02 V for **1** and 0.99 V for **2**, respectively. From the onset of oxidation/reduction potentials, the HOMO, LUMO, and HOMO-LUMO gap levels of these two complexes were obtained. The HOMO levels of **1** and **2** are -5.82 and -5.79 eV, respectively, indicating that the thiophen-2-yl replacing phenyl in the cyclometalated ligand could destabilize the HOMO level of complex **2**. That is because the HOMO orbitals of the cyclometalated iridium complexes generally reside on the iridium center and the coordinated phenyl moiety, thus the replacement of the phenyl ring by the electron-rich thiophen-2-yl moiety could help destabilize HOMO level. However, the LUMO levels of these two complexes are very close (-3.40 vs. -3.41 eV). Thus complex **2** have a little smaller energy gap (2.38 eV) than **1** (2.42 eV) due to the electronegativity of dtbpa is stronger than dpbpa. These results were further supported by the DFT and TDDFT calculations (see below).

Theoretical calculations

To gain further insight into the above photophysical and electrochemical properties of these two complexes, DFT and TD-DFT calculations were used to assess the frontier orbitals and electronic structures of these two complexes, particularly compared with the analogous 1,4-diphenylphthalazine based complex $[\text{Ir}(\text{dppa})_2(\text{Bphen})]^+\text{PF}_6^-$ and benzo[*g*]quinoline based complex $[\text{Ir}(\text{pbq-g})_2(\text{Bphen})]^+\text{PF}_6^-$ (**3**).²² As shown in Fig. 3, in comparison with $[\text{Ir}(\text{dppa})_2(\text{Bphen})]^+\text{PF}_6^-$, complex **1** and **2** show significantly destabilized HOMO orbitals (by 0.10 and 0.17 eV) and stabilized LUMO orbitals (by 0.06 and 0.14 eV), thus giving expected narrowed energy gaps for NIR-emission. That result suggests that the phenyl ring fused at *g* site in benzo[*g*]phthalazine ligands does effectively extend the π conjugated system of the parent phthalazine and the electron-rich thiophen-2-yl moieties could further help narrow the energy gap, which are in good agreement with the above photophysical and electrochemical results.

Meanwhile, complexes **1** and **2** have nearly equal Ir-C and Ir-N bond lengths to that of $[\text{Ir}(\text{dppa})_2(\text{Bphen})]^+\text{PF}_6^-$, indicating the benzo[*g*]phthalazine ligands does not bring extra steric hindrance as benzo[*g*]quinoline ligand in complex **3**. The calculated Ir-C bond lengths of complex **1** and **2** (2.01 Å and 2.00 Å, respectively) are almost same to those of complex **3** (2.00 Å)

Table 1 Photophysical and electrochemical characteristics of complexes **1** and **2** (compared with $[\text{Ir}(\text{pbq-g})_2(\text{Bphen})]^+\text{PF}_6^-$ (**3**))

	Absorption ^a	Room temperature emission ^b							
		CH_2Cl_2 solution			PMMA solid		Electrochemical data ^c		
		λ [nm] (ϵ [$\times 10^4 \text{ M}^{-1} \text{ cm}^{-1}$])	λ (nm)	Φ_{PL} (%)	τ (μs)	λ (nm)	Φ_{PL} (%)	$E_{\text{ox}}^{1/2}$ (V)	$E_{\text{red}}^{1/2}$ (V)
1	350 (3.6), 419 (1.8), 448 (1.5), 516 (0.6)	715, 788	3.1	0.79	708, 778	6.1	1.02	-1.40 , -1.55	2.42
2	321 (4.2), 421 (1.4), 454 (1.3), 535 (0.9)	775	2.9	0.33	760	4.1	0.99	-1.39 , -1.55	2.38
3 (ref. 22)	309 (7.7), 383 (1.9), 436 (1.1), 493 (0.5)	698, 760	3.5	1.86	700, 764	4.0	0.99	-1.60 , -1.74	2.60

^a In CH_2Cl_2 solutions (10^{-5} M). ϵ denotes the molar extinction coefficients. ^b In degassed CH_2Cl_2 (1×10^{-5} M) solutions. Φ_{PL} was measured using an absolute PL quantum yield measurement system. ^c Collected in CH_3CN solutions (10^{-3} M). The data were versus Fc^+/Fc (Fc is ferrocene). ^d $E_g = E_{\text{ox}}^{1/2} - E_{\text{red}}^{1/2}$.

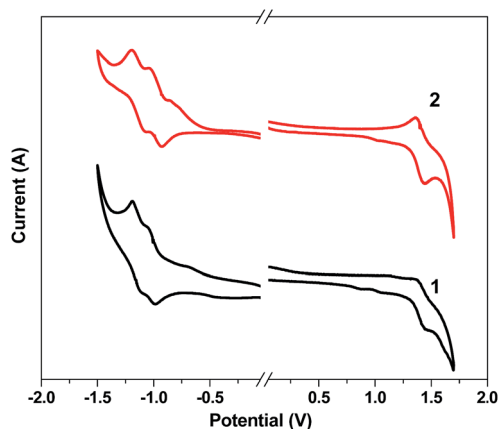


Fig. 2 Cyclic voltammograms of complexes 1 and 2 in anhydrous CH_3CN solutions (10^{-3} M) at a scan rate of 150 mV s^{-1} .

and $[\text{Ir}(\text{dppa})_2(\text{Bphen})]^+\text{PF}_6^-$. However, the calculated Ir–N bond lengths (2.06 Å and 2.07 Å, respectively) are clearly shorter than that of complex 3 (2.14 Å), indicating a stronger Ir–N bond in the complexes based on cyclometalated benzo[g]phthalazine derivatives. Such stronger Ir–N bonding results in stronger bonding between metal and ligand, which might lead to efficient mixing of the singlet and triplet excited states and be beneficial for

phosphorescence. Moreover, the dihedral angle between cyclometalated ligands and diimine ancillary ligand of complex 1 and 2 (89° and 89° , respectively) is about 10° greater than that of complex 3 (79°), which help loosen the steric hindrance toward the N chelating to the metal, thus improving the molecular stability and the whole phosphorescence of the complexes.³³

Complexes 1 and 2 show similar HOMO and LUMO configurations. The HOMO orbital resides on the iridium center and the coordinated phenyl or thiophen-2-yl moiety of the cyclometalated ligands, and the LUMO orbital dominates the benzo[g]phthalazine groups of the cyclometalated ligands. The calculated HOMO and LUMO energy levels are in accordance with the experimentally values from the CV measurements. To note, the ancillary ligand of Bphen has little contribution to the first two LUMOs of these two complexes. In contrast, for the cationic iridium complexes based on parent phthalazine and benzo[g]quinoline, their LUMOs are dominantly located on the ancillary ligand of Bphen. That indicates that the cyclometalated benzo[g]phthalazine ligand has better electron-accepting capability than the benzo[g]quinoline ligand and Bphen, which in good agreement with the relatively lowered the reduction potential ($\sim 0.2 \text{ eV}$) of the corresponding complexes.²²

Table 2 lists the vertical excitation energies and molecular orbitals involved in the excitations for the first two triplets. All

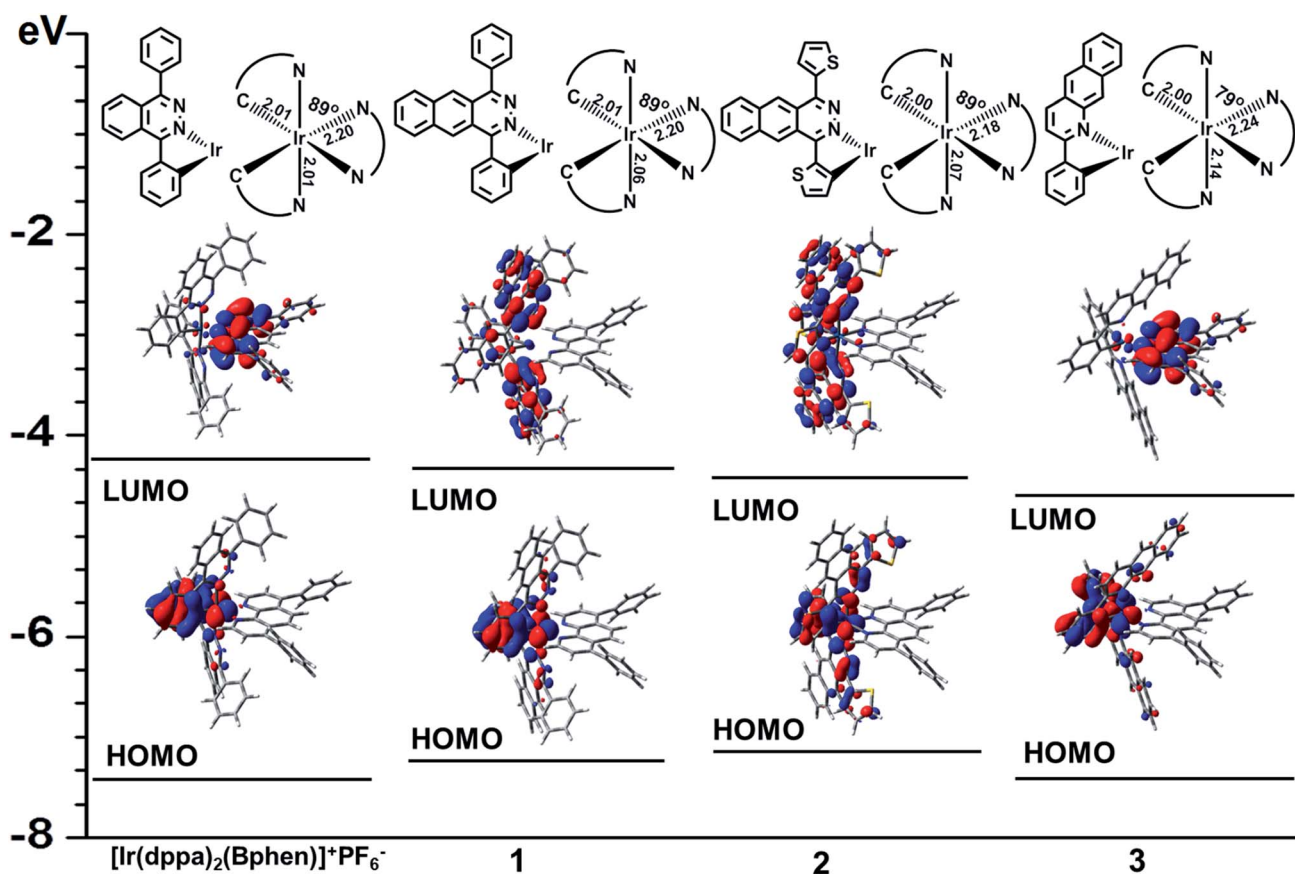


Fig. 3 The molecular structures, calculated bonding lengths, and the energy levels and isocontour plots of the frontier orbitals of complexes $[\text{Ir}(\text{dppa})_2(\text{Bphen})]^+\text{PF}_6^-$ (1) and $[\text{Ir}(\text{dtbpa})_2(\text{Bphen})]^+\text{PF}_6^-$ (2) compared with $[\text{Ir}(\text{dppa})_2(\text{Bphen})]^+\text{PF}_6^-$ and $[\text{Ir}(\text{pbq-g})_2(\text{Bphen})]^+\text{PF}_6^-$ (3).²² All the molecular surfaces correspond to an isocontour value of $|\psi| = 0.03$.

the complexes exhibit degenerate T_1 and T_2 states in energy. $[\text{Ir}(\text{dppa})_2(\text{Bphen})]^+\text{PF}_6^-$ based on the parent phthalazine ligand has the highest triplet energies about 2.19 eV and correspond to the transitions at 565 and 563 nm. In comparison, complexes **1** and **2** show significantly reduced triplet energies (by 0.44 and 0.58 eV), which correspond to a very large red shift around 140 nm due the highly conjugated cyclometalated benzo[*g*]phthalazine ligands. Their electron transitions correspond to 705 nm for **1** and 768 nm for **2**, which are very close to the experimentally observed emission peaks. All these electron transitions have a multi-configurational characteristic and dominantly originate from triplet metal-to-ligand charge transfer ($^3\text{MLCT}$, $d_\pi(\text{Ir}) \rightarrow \pi^*_{\text{C}^{\wedge}\text{N}}$) and intraligand charge transfer ($^3\text{ILCT}$, $\pi_{\text{C}^{\wedge}\text{N}} \rightarrow \pi^*_{\text{C}^{\wedge}\text{N}}$) as well as that of $[\text{Ir}(\text{dppa})_2(\text{Bphen})]^+\text{PF}_6^-$. In contrast, the analogous iridium complexes (**3**) based benzo[*g*]quinoline still have considerable contribution from $^3\text{MLCT}$ ($d_\pi(\text{Ir}) \rightarrow \pi^*_{\text{N}^{\wedge}\text{N}}$) and triplet ligand-ligand-charge-transfer ($^3\text{LLCT}$, $\pi_{\text{C}^{\wedge}\text{N}} \rightarrow \pi^*_{\text{N}^{\wedge}\text{N}}$), thus in most cases rendering relatively lower PLQY than the mixed MLCT and ILCT emitting materials. That mixing of $^3\text{MLCT}$ and $^3\text{ILCT}$ in complexes **1** and **2** might play an important role for nice PLQY because this intersystem crossing can be enhanced for the systems involved notable MLCT participation.³⁴

Electrophosphorescent devices

The NIR-emitting OLEDs based on complexes **1** and **2** were fabricated by spin-coating and vacuum thermal evaporation, with the configuration of ITO/PEDOT:PSS (40 nm)/poly(vinylcarbazole)

(PVK): 2-(4-biphenyl)-5-(4-*tert*-butylphenyl)-1,3,4-oxadiazole (PBD, 30 wt%): **1** or **2** (10–20 wt%) (90 nm)/TPBI (30 nm)/ Cs_2CO_3 (2.3 nm)/Al (150 nm). The PVK–PBD blend was used as the host material because of its desirable bipolar character and good film-forming capability through solution process. TPBI was used as the electron-transporting and exciton-blocking layer. The doping concentration of complexes **1** and **2** varied from 10 to 20 wt% to optimize the device performance. As shown in Fig. 4a, the emission from the host around 415 nm can be nearly quenched when the doping concentration increased to 20 wt% and the intense NIR emission was detected at 715 nm, 788 nm for the devices with complex **1** and 791 nm for the devices with complex **2**. Interestingly, for the devices with complex **1**, the emission band at the long wavelength of 788 nm exhibited much stronger intensity than that at short wavelength of 715 nm, which is very different from the PL spectra of complex **1**.

Furthermore, the emission intensity at long wavelength increases as the doping concentration increases. That might be ascribed to the optical effects in devices or the confined radiation field by the metal cathode.³⁵ For the devices with complex **2**, there is a small peak at 580 nm at 10 wt% doping concentration, which could be tentatively attributed to the emission from the possible interface exciplex between PVK and TPBI. That suggests complex **2** with electron-rich thiophen-2-yl moieties might contribute to hole transport and help move the recombination zone approaching the interface between host and TPBI. The underlying mechanism needs further investigation. When the doping concentration increases to 20 wt%, the visible

Table 2 The first two triplet states for complexes **1** and **2** (compared with $[\text{Ir}(\text{dppa})_2(\text{Bphen})]^+\text{PF}_6^-$ and $[\text{Ir}(\text{pbq-g})_2(\text{Bphen})]^+\text{PF}_6^-$ **3**) calculated using the TDDFT approach

Complexes	States (E (eV), λ^a (nm))	Dominant excitations ^b	Character
$[\text{Ir}(\text{dppa})_2(\text{Bphen})]^+\text{PF}_6^-$	T_1 (2.194, 565)	H → L+2 (0.54) H-1 → L+3 (0.27) H-2 → L+2 (0.11)	$\pi(\text{Bppa})/d_\pi(\text{Ir}) \rightarrow \pi^*(\text{Bppa})$ $\pi(\text{Bppa})/d_\pi(\text{Ir}) \rightarrow \pi^*(\text{Bppa})$ $\pi(\text{Bppa})/d_\pi(\text{Ir}) \rightarrow \pi^*(\text{Bppa})$
	T_2 (2.199, 563)	H → L+3 (0.47) H-1 → L+2 (0.34) H-2 → L+3 (0.12)	$\pi(\text{Bppa})/d_\pi(\text{Ir}) \rightarrow \pi^*(\text{Bppa})$ $\pi(\text{Bppa})/d_\pi(\text{Ir}) \rightarrow \pi^*(\text{Bppa})$ $\pi(\text{Bppa})/d_\pi(\text{Ir}) \rightarrow \pi^*(\text{Bppa})$
1	T_1 (1.758, 705)	H-1 → L (0.50) H-2 → L+1 (0.27) H → L+1 (0.22)	$\pi(\text{dppba})/d_\pi(\text{Ir}) \rightarrow \pi^*(\text{dppba})$ $\pi(\text{dppba})/d_\pi(\text{Ir}) \rightarrow \pi^*(\text{dppba})$ $\pi(\text{dppba})/d_\pi(\text{Ir}) \rightarrow \pi^*(\text{dppba})$
	T_2 (1.758, 705)	H-1 → L+1 (0.48) H-2 → L (0.28) H → L (0.24)	$\pi(\text{dppba})/d_\pi(\text{Ir}) \rightarrow \pi^*(\text{dppba})$ $\pi(\text{dppba})/d_\pi(\text{Ir}) \rightarrow \pi^*(\text{dppba})$ $\pi(\text{dppba})/d_\pi(\text{Ir}) \rightarrow \pi^*(\text{dppba})$
2	T_1 (1.613, 768)	H → L (0.56) H-1 → L+1 (0.39) H-2 → L (0.04)	$\pi(\text{dtbpa})/d_\pi(\text{Ir}) \rightarrow \pi^*(\text{dtbpa})$ $\pi(\text{dtbpa})/d_\pi(\text{Ir}) \rightarrow \pi^*(\text{dtbpa})$ $\pi(\text{dtbpa})/d_\pi(\text{Ir}) \rightarrow \pi^*(\text{dtbpa})$
	T_2 (1.622, 764)	H → L+1 (0.48) H-1 → L (0.46) H-2 → L+1 (0.05)	$\pi(\text{dtbpa})/d_\pi(\text{Ir}) \rightarrow \pi^*(\text{dtbpa})$ $\pi(\text{dtbpa})/d_\pi(\text{Ir}) \rightarrow \pi^*(\text{dtbpa})$ $\pi(\text{dtbpa})/d_\pi(\text{Ir}) \rightarrow \pi^*(\text{dtbpa})$
3 (ref. 22)	T_1 (1.789, 693)	H-2 → L+2 (0.24) H-1 → L+3 (0.20) H-1 → L+1 (0.16)	$\pi(\text{pbq-g})/d_\pi(\text{Ir}) \rightarrow \pi^*(\text{pbq-g})$ $\pi(\text{pbq-g})/d_\pi(\text{Ir}) \rightarrow \pi^*(\text{pbq-g})/\pi^*(\text{Bphen})$ $\pi(\text{pbq-g})/d_\pi(\text{Ir}) \rightarrow \pi^*(\text{pbq-g})$
	T_2 (1.791, 692)	H-1 → L+2 (0.32) H-2 → L+3 (0.15) H-2 → L+1 (0.12)	$\pi(\text{pbq-g})/d_\pi(\text{Ir}) \rightarrow \pi^*(\text{pbq-g})$ $\pi(\text{pbq-g})/d_\pi(\text{Ir}) \rightarrow \pi^*(\text{pbq-g})/\pi^*(\text{Bphen})$ $\pi(\text{pbq-g})/d_\pi(\text{Ir}) \rightarrow \pi^*(\text{pbq-g})$

^a Data in parentheses are excitation energies and corresponding wavelengths. ^b H and L denote HOMO and LUMO, respectively; data in parentheses are the contributions of corresponding excitations.

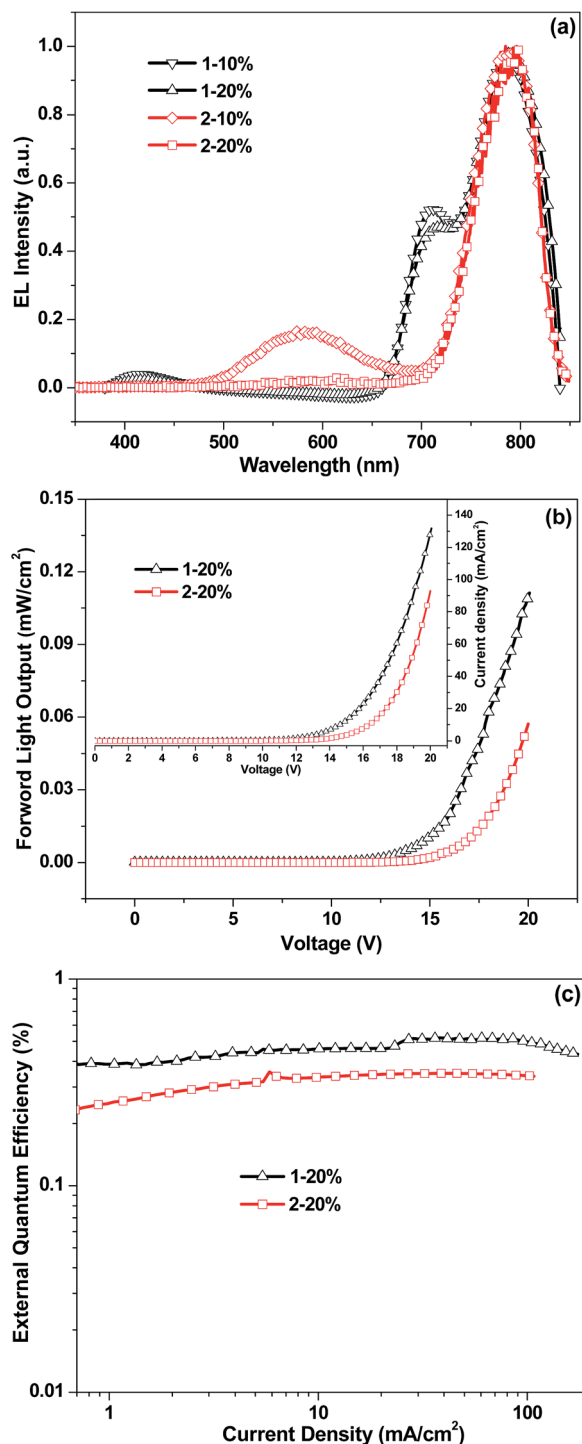


Fig. 4 Characteristics of OLEDs based complex 1 and 2. (a) Electroluminescent spectra at the driving voltage of 14 V. (b) Forward light output vs. bias voltage and current density vs. bias voltage (inset) characteristics. (c) External quantum efficiency vs. current density characteristics.

emission is nearly quenched and the NIR emission at 791 nm is detected. That implies complete energy transfer from the host and interface exciplex to the dopants.³⁶

At the doping concentration of 20 wt%, the devices exhibited the best performances with a constant EQE about 0.50%, and

the maximum forward light output of 1112 and 572 $\mu\text{W m}^{-2}$ at 20 V for complexes 1 and 2, respectively (Fig. 4b and c). It is worth noting that the devices exhibited negligible efficiency roll-off with increasing current density. Even at 100 mA cm^{-2} , the value of EQE still remained at 0.50% and 0.34% for the devices with complexes 1 and 2, respectively. Just like our previously reported NIR-emitting iridium complexes,^{19–21} this result again corroborated that iridium complexes would endow the NIR-OLEDs with the unique characteristics of negligible efficiency roll-off.

Conclusions

In summary, we have designed and synthesized two novel NIR-emitting cationic iridium complexes based on highly conjugated cyclometalated benzo[g]phthalazine ligands, with bathochromically shifted emission up to 775 nm and notable PLQY up to 6.1% in solid films. Density functional theory calculations have been carried out to reveal that the newly cyclometalated benzo[g]phthalazine ligands have several advantages over the previous benzo[g]quinoline ligands, including much stronger Ir–N bonds, less chelate congestion, better electron-accepting ability, thus providing the corresponding complexes with satisfactory NIR emissions due to the desirable MLCT mixed with ILCT. Employing these two complexes, the NIR-OLEDs have been fabricated and showed nearly flat efficiency-current density characteristics with the EQE around 0.5% over a wide range of current density of 1–100 mA cm^{-2} . Such unique characteristics allow great potential of NIR-emitting iridium complexes for practical applications. To further improve the device efficiency, the synthesis of the corresponding neutral complexes and optimization of the device structures are underway.

Acknowledgements

We thank the National Nature Science Foundation of China (no. 51473086 and 21161160447) and the National Key Basic Research and Development Program of China (no. 2011CB808403) for financial support. We especially thank Professor Hua Ruimao and Senior engineer Jianhua Cao for their help to synthesize the benzo[g]phthalazine ligands.

Notes and references

- 1 G. Qian and Z. Y. Wang, *Chem.-Asian. J.*, 2010, **5**, 1006–1029.
- 2 J. O. Escobedo, O. Rusin, S. Lim and R. M. Strongin, *Curr. Opin. Chem. Biol.*, 2010, **14**, 64–70.
- 3 H. Xiang, J. Cheng, X. Ma, X. Zhou and J. J. Chruma, *Chem. Soc. Rev.*, 2013, **42**, 6128–6185.
- 4 C.-L. Ho, H. Li and W.-Y. Wong, *J. Org. Chem.*, 2014, **751**, 261–285.
- 5 J.-C. G. Bünzli, *Chem. Rev.*, 2010, **110**, 2729–2755.
- 6 S. V. Eliseeva and J.-C. G. Bünzli, *Chem. Soc. Rev.*, 2010, **39**, 189–227.
- 7 R. Yang, R. Tian, J. Yan, Y. Zhang, J. Yang, Q. Hou and Y. Cao, *Macromolecules*, 2005, **38**, 244–253.

- 8 B. C. Thompson, L. G. Madrigal, M. R. Pinto, T. S. Kang, K. S. Schanze and J. R. Reynolds, *Polym. Chem.*, 2005, **43**, 1417–1431.
- 9 S. C. Moratti, R. Cervini, A. B. Holmes, D. R. Baigent, R. H. Friend, N. C. Greenham, J. Grt er and P. J. Hamer, *Synth. Met.*, 1995, **71**, 2117–2120.
- 10 C. Borek, K. Hanson, P. I. Djurovich, M. E. Thompson, K. Aznavour, R. Bau, Y. Sun, S. R. Forrest, J. Brooks, L. Michalski and J. Brown, *Angew. Chem.*, 2007, **119**, 1127–1130.
- 11 J. R. Sommer, R. T. Farley, K. R. Graham, Y. Yang, J. R. Reynolds, J. Xue and K. S. Schanze, *ACS Appl. Mater. Interfaces*, 2009, **1**, 274–278.
- 12 K. R. Graham, Y. X. Yang, J. R. Sommer, A. H. Shelton, K. S. Schanze, J. G. Xue and J. R. Reynolds, *Chem. Mater.*, 2011, **23**, 5305–5312.
- 13 J. Kalinowski, V. Fattori, M. Cocchi and J. A. G. Williams, *Coord. Chem. Rev.*, 2011, **255**, 2401–2415.
- 14 E. L. Williams, J. Li and G. E. Jabbour, *Appl. Phys. Lett.*, 2006, **89**, 083506.
- 15 H.-Y. Chen, C.-H. Yang, Y. Chi, Y.-M. Cheng, Y.-S. Yeh, P.-T. Chou, H.-Y. Hsieh, C.-S. Liu, S.-M. Peng and G.-H. Lee, *Can. J. Chem.*, 2006, **84**, 309–318.
- 16 X. Cao, J. Miao, M. Zhu, C. Zhong, C. Yang, H. Wu, J. Qin and Y. Cao, *Chem. Mater.*, 2015, **27**, 96–104.
- 17 T. C. Lee, J. Y. Hung, Y. Chi, Y. M. Cheng, G. H. Lee, P. T. Chou, C.-C. Chen, C.-H. Chang and C. C. Wu, *Adv. Funct. Mater.*, 2009, **19**, 2639–2647.
- 18 T. Yu, D. P.-K. Tsang, V. K.-M. Au, W. H. Lam, M.-Y. Chan and V. W.-W. Yam, *Chem.–Eur. J.*, 2013, **19**, 13418–13427.
- 19 J. Qiao, L. Duan, L. Tang, L. He, L. Wang and Y. Qiu, *J. Mater. Chem.*, 2009, **19**, 6573–6580.
- 20 R. Tao, J. Qiao, G. Zhang, L. Duan, L. D. Wang and Y. Qiu, *J. Phys. Chem. C*, 2012, **116**, 11658–11664.
- 21 R. Tao, J. Qiao, G. Zhang, L. Duan, C. Chen, L. Wang and Y. Qiu, *J. Mater. Chem. C*, 2013, **1**, 6446–6454.
- 22 G. Zhang, H. Zhang, Y. Gao, R. Tao, L. Xin, J. Yi, F. Li, W. Liu and J. Qiao, *Organometallics*, 2014, **33**, 61–68.
- 23 J. A. Clement and A. K. Mohanakrishnan, *Tetrahedron*, 2010, **66**, 2340–2350.
- 24 M. J. Haddadin, B. J. Agha and R. F. Tabri, *J. Org. Chem.*, 1979, **44**, 494–497.
- 25 M. J. Frisch, G. W. Trucks, H. B. Schlegel, G. E. Scuseria, M. A. Robb, J. R. Cheeseman, J. A. Montgomery Jr, T. Vreven, K. N. Kudin, J. C. Burant, J. M. Millam, S. S. Iyengar, J. Tomasi, V. Barone, B. Mennucci, M. Cossi, G. Scalmani, N. Rega, G. A. Petersson, H. Nakatsuji, M. Hada, M. Ehara, K. Toyota, R. Fukuda, J. Hasegawa, M. Ishida, T. Nakajima, Y. Honda, O. Kitao, H. Nakai, M. Klene, X. Li, J. E. Knox, H. P. Hratchian, J. B. Cross, V. Bakken, C. Adamo, J. Jaramillo, R. Gomperts, R. E. Stratmann, O. Yazyev, A. J. Austin, R. Cammi, C. Pomelli, J. W. Ochterski, P. Y. Ayala, K. Morokuma, G. A. Voth, P. Salvador, J. J. Dannenberg, V. G. Zakrzewski, S. Dapprich, A. D. Daniels, M. C. Strain, O. Farkas, D. K. Malick, A. D. Rabuck, K. Raghavachari, J. B. Foresman, J. V. Ortiz, Q. Cui, A. G. Baboul, S. Clifford, J. Cioslowski, B. B. Stefanov, G. Liu, A. Liashenko, P. Piskorz, I. Komaromi, R. L. Martin, D. J. Fox, T. Keith, M. A. Al-Laham, C. Y. Peng, A. Nanayakkara, M. Challacombe, P. M. W. Gill, B. Johnson, W. Chen, M. W. Wong, C. Gonzalez and J. A. Pople, *Gaussian 03*, Gaussian, Inc., Wallingford, CT, 2004.
- 26 C. T. Lee, W. T. Yang and R. G. Parr, *Phys. Rev. B: Condens. Matter Mater. Phys.*, 1988, **37**, 785–789.
- 27 A. J. Becke, *Chem. Phys.*, 1993, **98**, 5648–5652.
- 28 Y.-J. Su, H.-L. Huang, C.-L. Li, C.-H. Chien, Y.-T. Tao, P.-T. Chou, S. Datta and R.-S. Liu, *Adv. Mater.*, 2003, **15**, 884–888.
- 29 A. Tsuboyama, H. Iwawaki, M. Furugori, T. Mukaide, J. Kamatani, S. Igawa, T. Moriyama, S. Miura, T. Takiguchi, S. Okada, M. Hoshino and K. Ueno, *J. Am. Chem. Soc.*, 2003, **125**, 12971–12979.
- 30 F.-I. Wu, H.-J. Su, C.-F. Shu, L. Luo, W.-G. Diao, C.-H. Cheng, J.-P. Duan and G.-H. Lee, *J. Mater. Chem.*, 2005, **15**, 1035–1042.
- 31 Z. Q. Gao, B. X. Mi, H. L. Tam, K. W. Cheah, C. H. Chen, M. S. Wong, S. T. Lee and C. S. Lee, *Adv. Mater.*, 2008, **20**, 774–778.
- 32 B. Tong, Q. Mei, S. Wang, Y. Fang, Y. Meng and B. Wang, *J. Mater. Chem.*, 2008, **18**, 1636–1639.
- 33 B. X. Mi, P. F. Wang, Z. Q. Gao, C. S. Lee, S. T. Lee, H. L. Hong, X. M. Chen, M. S. Wong, P. F. Xia, K. W. Cheah, C. H. Chen and W. Huang, *Adv. Mater.*, 2009, **21**, 339–343.
- 34 P. T. Chou and Y. Chi, *Chem.–Eur. J.*, 2007, **13**, 380–395.
- 35 D. Song, S. Zhao and H. Aziz, *Adv. Funct. Mater.*, 2011, **21**, 2311–2317.
- 36 Y.-S. Park, W.-I. Jeong and J.-J. Kim, *J. Appl. Phys.*, 2011, **110**, 124519.